

Computer simulation of the phase diagram for a fluid confined in a fractal and disordered porous material

V. De Grandis[†], P. Gallo[†] and M. Rovere^{†*}

[†] *Dipartimento di Fisica, Università “Roma Tre”,
INFM and Democritos National Simulation Center,
Via della Vasca Navale 84, 00146 Roma, Italy.*

Abstract

We present a grand canonical Monte Carlo simulation study of the phase diagram of a Lennard-Jones fluid adsorbed in a fractal and highly porous aerogel. The gel environment is generated from an off-lattice diffusion limited cluster-cluster aggregation process. Simulations have been performed with the multicanonical ensemble sampling technique. The biased sampling function has been obtained by histogram reweighting calculations. Comparing the confined and the bulk system liquid-vapor coexistence curves we observe a decrease of both the critical temperature and density in qualitative agreement with experiments and other Monte Carlo studies on Lennard-Jones fluids confined in random matrices of spheres. At variance with these numerical studies we do not observe upon confinement a peak on the liquid side of the coexistence curve associated with a liquid-liquid phase coexistence. In our case only a shouldering of the coexistence curve appears upon confinement. This shoulder can be associated with high density fluctuations in the liquid phase. The coexisting vapor and liquid phases in our system show a high degree of spatial disorder and inhomogeneity.

PACS numbers: 61.20.Ja, 64.70.Fx, 05.70.Fh

I. INTRODUCTION

The phase behavior of fluids and fluid mixtures confined in porous and disordered materials represents a field of continuing theoretical and experimental interest due to a variety of applications in industrial technology¹. For example, porous materials are employed as adsorbents in many industrial processes, such as catalysis, adsorption separation, filtration and purification.

Experimental studies on the phase behavior of fluids adsorbed both in highly porous materials, such as silica aerogels^{2,3,4,5,6,7}, and in less porous ones, such as Vycor glasses^{8,9,10,11,12,13}, have been performed. All these studies have shown that the phase diagram of the fluids confined in the porous structures is strongly altered in comparison with the corresponding bulk systems. For $^4\text{He}^3$ and N_2^6 confined in very dilute aerogels it has been found that the liquid-vapor coexistence curve is much narrower and the critical temperature is lower than in the bulk. It has also been observed a shift of the critical density towards the liquid phase and an increase of the coexistence vapor phase densities attributed to the attractive fluid-gel interactions.

Very few theoretical studies on fluids confined in disordered porous materials have been performed. A theoretical approach based on considering the gel as a random field acting on the fluid succeeded in reproducing the important feature of spatial inhomogeneity¹⁴. Important phenomena like wetting cannot nonetheless be reproduced by such model. A model of “quenched-annealed” binary mixture was first studied by Madden and Glandt¹⁵ and then widely used in dealing with the

problem of fluids phase separation in porous materials. Following this model, several integral equation theories and computer simulation studies have been successively proposed, in which the porous material is described by a random matrix of spheres^{16,17,18,19,20}.

In particular the simulation work done by Page and Monson¹⁹ dealt with the calculation of the phase diagram for a system representative of methane adsorbed in a silica xerogel and that of Alvarez and al.²⁰ has investigated the sensitivity of the confined fluid phase behavior to the matrix realization. The results of these studies about the vapor-liquid coexistence curve are in good qualitative agreement with experiments. The novelty of these works not observed in experiments is the occurrence of an additional phase transition between a medium density liquid and an high density one. The liquid-liquid phase coexistence has been associated with the wetting properties of the fluid in the more dense regions of the adsorbent. This second phase transition however has been found to be very sensitive to the matrix realization, while the liquid-vapor coexistence properties are seen to be robust to variations in the solid structure^{20,21}. This behavior has been explained observing that the additional liquid-liquid transition is associated with the filling of low porosity regions in the matrix, which can occur for some configurations but not for others. The picture which emerges from all these calculations is that the coexistence vapor and liquid phases for the confined fluids are disordered and inhomogeneous as a consequence of the adsorbent structure randomness.

The description of the aerogel as a random matrix of spheres however is not sufficiently realistic. The gel is organized into a fractally correlated structure experimentally identified by a strong diffraction peak at small wave vectors measured by small angle x-ray or neutron scattering^{22,23,24,25}. The fractal behavior of aerogels is associated with the irreversibility of the gel formation dy-

*Author to whom correspondence should be addressed; e-mail: rovere@fis.uniroma3.it

namics, which proceed by random colloidal aggregation of silica particles. The fractal dimension of silica aerogels is about 1.80 in three dimensions²⁴.

Structures with similar fractal dimension have been generated by Monte Carlo simulations using several hierarchical cluster-cluster algorithms^{24,25,26}. In particular the Diffusion Limited Cluster-Cluster Aggregation procedure (DLCA) is a gel growth process widely used in theoretical studies of aerogels^{25,27}. It has been shown that the structural properties and fractal dimension of DLCA gels well agree with experimental data on silica aerogels. A theoretical study of thermodynamical and structural properties of a Lennard-Jones fluid adsorbed in a highly porous DLCA aerogel by means of an integral equation approach has been recently proposed¹⁷. The phase diagram as well as the structural correlations of the confined fluid are found to be influenced by the specific properties of the gel, such as its connectivity and fractal behavior, particularly at low fluid densities. These results support the idea that a realistic modeling of the gel environment is necessary to deeply investigate the effects of the porous medium structural properties on the phase behavior of the adsorbate, especially on the second disorder-induced liquid-liquid transition.

In this paper we present the results of a grand canonical Monte Carlo simulation study about the phase behavior of a Lennard-Jones fluid confined in a dilute DLCA aerogel, where fluid and gel particles have hard core diameters of equal size and interact by means of an hard sphere potential. In order to locate the liquid-vapor coexistence curve we have calculated the density distribution functions. The multicanonical ensemble sampling (MES) procedure has been employed to investigate thermodynamical states in the subcritical region^{28,29,30}. In the next section we describe the algorithm to build our confining system. In Sec. 3 we give details of our simulation. In Sec. 4 we present the results about the confined fluid phase diagram and compare it with that of the bulk system. Sec. 5 is devoted to conclusions.

II. CONFINING SYSTEM

The algorithm we used to generate the aerogel configuration is the three dimensional off-lattice extension by Hasmy and al.²⁵ of the DLCA procedure first proposed by Kolb and Hermann²⁷. The DLCA process is an iterative method which starts with a collection of N identical spherical particles of diameter σ_a randomly placed in a cubic box of side L , with volume fraction $\eta = \frac{\pi}{6} \sigma_a^3 \frac{N}{L^3}$. Aggregation proceeds via a diffusion motion of the particles.

If during their motion two clusters collide they stick together forming a new single aggregate. The process is terminated when a single cluster is obtained. Periodic boundary conditions are used at the edges of the simulation box. Details of the DLCA algorithm can be found in references^{25,27}. We have generated with this algorithm

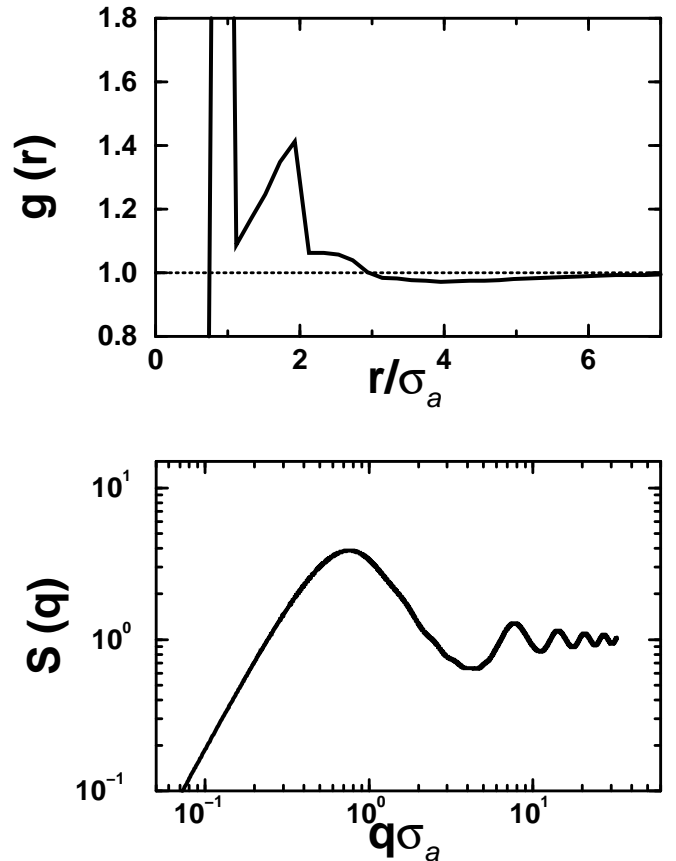


FIG. 1: On the top plot of $g(r)$ versus r/σ_a for an aerogel containing 515 particles in a box of edge $L = 15\sigma_a$. This curve results from an average of 50 simulations. On the bottom Log-Log plot of $S(q)$ versus $q\sigma_a$.

configurations for aerogels containing 515 particles in a box of edge $L = 15\sigma_a$, corresponding to a volume fraction $\eta = 0.08$ and a porosity P , defined as the ratio between the free space volume and the volume occupied by the gel, of 92%.

We have calculated for these aggregates the radial distribution function $g(r)$ and the static structure factor $S(q)$ following the lines of the simulation work by Hasmy and al.²⁵ Our results are reported in Fig. 1. The radial distribution function $g(r)$ presents a strong peak at $r = \sigma_a$, associated with bonds between contacting particles, and other features corresponding to short range correlations between particles belonging to the same cluster (see references^{24,25} for further details). Before reaching the asymptotic limit of 1, $g(r)$ exhibits a minimum corresponding to distances between particles located at the boundary of the clusters. The location of this minimum gives an estimate of the mean clusters size ξ . In our case the mean cluster size is about $4\sigma_a$. As a consequence of the presence of the minimum in $g(r)$, the scattering function $S(q)$, which is related to the Fourier transform of $g(r) - 1$, exhibits a pronounced peak at small q . The gel

exhibits a fractal structure in the intermediate q -range. The fractal dimension can be estimated from the power law behavior of the scattering function, $S(q) \sim q^{-D}$ in this q -range. In our case we have obtained $D \sim 1.74$ consistent with the value expected for silica aerogels in three dimensions^{24,25}.

III. SIMULATION DETAILS

In our simulations the interactions between fluid particles are described by a Lennard-Jones potential with a collision diameter σ and a depth ϵ truncated at $r_c = 2.5\sigma$. The aerogel particles are quenched and interact with the fluid particles by means of a purely repulsive hard sphere potential. We assume that fluid particles have a collision diameter of the same size as the aerogel hard core $\sigma = \sigma_a$. The edge of our simulation box is $L = 15\sigma$. In the following Lennard-Jones units will be used: σ for lengths, ϵ for energies and ϵ/k_B for temperatures.

In order to study the phase diagram of the Lennard-Jones fluid we have carried out Monte Carlo simulations in the grand canonical ensemble^{31,32} employing the algorithm used by Wilding^{29,30}. MC moves consist of either an insertion or a deletion attempt, proposed with equal probability. Particles movements are implicitly implemented through insertion and deletion moves.

In order to calculate the liquid and vapor coexistence densities the chemical potential can be varied, at fixed temperature, until a bimodal shape of the particles number distribution $P(N)$ is obtained. The coexistence densities at the selected temperature correspond to the two peaks positions. To obtain also the location of the liquid-gas saturation line in the (μ, T) plane the equal peak weight criterion³⁰ can be applied. According to this criterion the chemical potential is tuned, at constant temperature, until the measured $P(N)$ is double-peaked with equal area under the two peaks. The corresponding chemical potential belongs to the fluid coexistence curve.

This conventional grand canonical ensemble Monte Carlo technique becomes however impractical in the subcritical region we are interested in, due to the large free energy barrier separating the two phases and hindering spontaneous fluctuations of the system from the liquid to the gas phase and viceversa. In order to enhance crossing of this free energy barrier we have used the recently proposed MES^{28,29,30}. With this powerful technique sampling is made from a non Boltzmann distribution, with a modified Hamiltonian $H' = H + g(N)$, where $H(\mathbf{r}, N) = E(\mathbf{r}) - \mu N$ is the configurational Hamiltonian. The biased sampling function $g(N)$ has to be chosen in such a way that the measured distribution $P'(N)$ is nearly flat. In this way the mixed-phase configurations will be sampled with approximately the same probability as the gas and liquid configurations. The best choice for the biased sampling function would be $g(N) = \ln P(N)$, where $P(N)$ is the distribution we are looking for. An estimate $\tilde{P}(N)$ can be obtained by extrapolation mak-

ing use of the histogram reweighting technique³³. In this approach we can accumulate the joint probability distribution of system energy and particles number for a thermodynamical state characterized by a temperature T_0 and a chemical potential μ_0 (near the critical point where the interfacial tension is low)²⁰:

$$P(N, E|T_0, \mu_0) = \frac{e^{-\frac{H_0}{kT_0}} \mathcal{D}}{\mathcal{Z}_0} \quad (1)$$

where $\mathcal{D}(N, E)$ is the density of states and $\mathcal{Z}_0(T_0, \mu_0)$ is the grand partition function. An estimate \tilde{P} of this distribution for another thermodynamical state (T_1, μ_1) can now be provided:

$$\tilde{P}(N, E|T_1, \mu_1) = \frac{\mathcal{Z}_0}{\mathcal{Z}_1} e^{-(\frac{H_1}{kT_1} - \frac{H_0}{kT_0})} P(N, E|T_0, \mu_0) \quad (2)$$

The new thermodynamical point (T_1, μ_1) has to be sufficiently close to (T_0, μ_0) in such a way that the statistical weight of the new configuration is not too different from the previous one. Integrating over the system energy E , we can finally obtain a suitable bias function :

$$\tilde{P}(N|T_1, \mu_1) = \int dE \tilde{P}(N, E|T_1, \mu_1) \quad (3)$$

At the end of the Monte Carlo simulation at (T_1, μ_1) with the biased Hamiltonian we obtain the almost flat $P'(N)$. The real particles number distribution $P(N)$ pertaining to (T_1, μ_1) is recovered from: $P(N) = P'(N) \cdot \tilde{P}(N)$.

This method has given more accurate results than the well known Gibbs ensemble technique and Gibbs-Duhem integration scheme both for bulk and confined fluids^{20,29}.

We have performed extensive MES simulations in order to calculate the confined fluid phase diagram for a range of subcritical temperatures from $T = 0.96$ to $T = 0.79$. Our simulations involved about $200 \cdot 10^6$ steps for system equilibration and, depending on temperature, from $1 \cdot 10^9$ to $2 \cdot 10^9$ steps for calculating the ensemble averages.

Runs of this order of magnitude are necessary in order to supply enough independent samples from each of the two phases and consequently obtain density distribution functions with enough accuracy for our analysis³⁰. We note that on decreasing temperature the rate of the interchanges between the liquid and gas phases becomes more rare and longer runs are needed.

IV. RESULTS

A. Simulation in the two-phase region

First of all we need to locate the coexistence curve of the confined fluid and in particular the near-critical region. For this sake we have calculated with standard grand canonical simulations adsorption isotherms of the

density ρ versus the chemical potential μ for temperatures ranging from $T = 0.80$ to $T = 0.95$. Our results are shown in Fig. 2. FIGURA2 For a given temperature,

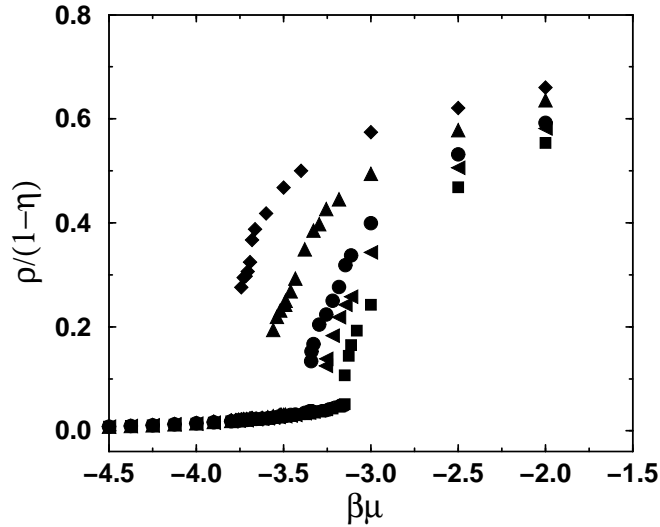


FIG. 2: Adsorption isotherms for a Lennard-Jones fluid in a DLCA aerogel for a range of subcritical temperatures ($T = 0.80$ diamonds, $T = 0.85$ triangles up, $T = 0.90$ circles, $T = 0.92$ triangles left and $T = 0.95$ squares). The fluid density has been normalized by the void fraction $(1 - \eta)$ of the simulation box volume, where η is the gel volume fraction. All quantities are in Lennard-Jones units.

we observe evidence of a coexistence at the same chemical potential between a dilute gas and a medium density liquid in our confined system. We have not observed in our isotherms the occurrence of a liquid-liquid phase coexistence, at variance with previous computer simulation studies on the phase behavior of Lennard-Jones fluids in disordered non fractal matrices of spheres^{19,20}.

In our calculations we have not considered desorption isotherms and the hysteresis associated usually with capillary condensation^{1,34} since we are interested in the coexistence between equilibrium phases.

We note that due to the slope of the liquid portion of the isotherms a small change of the chemical potential induces a strong variation in the liquid density. Therefore it is difficult to tune the chemical potential with the appropriate resolution to locate the coexisting densities with enough accuracy. On approaching the critical region this problem becomes even worst.

B. Multicanonical ensemble sampling

In order to better investigate the coexistence region and in particular the possible existence of a liquid-liquid phase coexistence we carried out extensive MES calculations.

From our isotherms calculations we have roughly estimated the region where the onset of the bimodal shape of

the particles number distribution $P(N)$ can be observed. In our analysis we started from the double-peaked $P(N)$ obtained at the temperature $T = 0.96$. The histogram reweighting technique allowed us to estimate the coexistence liquid and vapor densities and chemical potential at this temperature. Then by making use of the MES procedure we investigated a wide range of subcritical temperatures. In Fig. 3 we report the distributions $P(N)$ for the thermodynamical states investigated starting from $T = 0.96$.

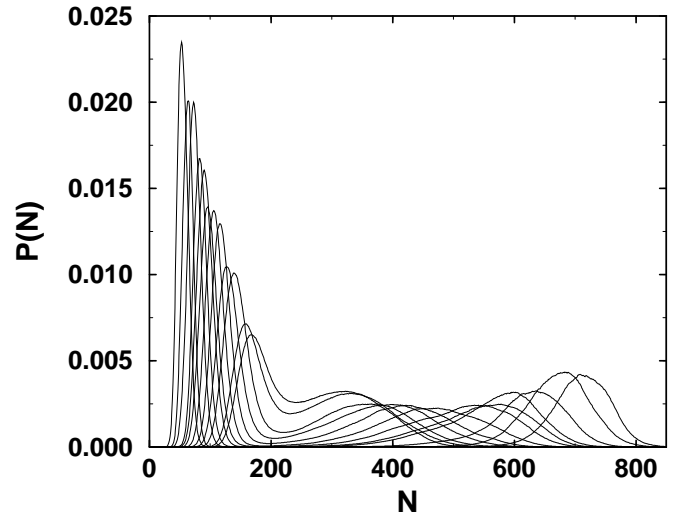


FIG. 3: Coexistence particles number distributions for subcritical temperatures ranging from $T = 0.96$ to $T = 0.79$ in Lennard-Jones units. Curves with closer peaks correspond to higher temperatures.

At higher temperatures the liquid and gas have close densities and the double-peaked $P(N)$ distribution shows two partially overlapped peaks. As the temperature decreases the difference between the coexisting vapor and liquid densities becomes more marked.

In the intermediate temperature regime we do not observe the occurrence of a third peak associated with a second coexisting liquid phase. We will comment more extensively about this point in the following. Table I summarizes the temperatures at which we performed our simulations together with the values of the coexistence densities. The MES algorithm allowed us to follow the system down to $T = 0.79$, where the liquid density is more than 10 times higher than the vapor one. Snapshots from our simulations for the coexistence liquid and vapor configurations at one temperature are shown in Fig. 4 and Fig. 5. In both the coexisting phases the spatial distribution of the fluid molecules is inhomogeneous and the pores of the aerogel are far from being uniformly filled by the fluid.

Fig. 6 shows the temperature versus density phase diagram we obtained from the peaks locations in the $P(N)$ distributions depicted in Fig. 3, compared with that of the bulk fluid²⁹. We find that the confined fluid phase

T	$\rho_g/(1-\eta)$	$\rho_l/(1-\eta)$
0.960	0.054	0.104
0.950	0.051	0.107
0.930	0.045	0.117
0.915	0.041	0.128
0.900	0.038	0.138
0.885	0.033	0.153
0.870	0.031	0.172
0.860	0.029	0.185
0.850	0.027	0.194
0.830	0.023	0.205
0.810	0.021	0.220
0.790	0.017	0.228

TABLE I: The peak densities corresponding to the number particles distributions shown in Fig. 3. All quantities are in Lennard-Jones units.

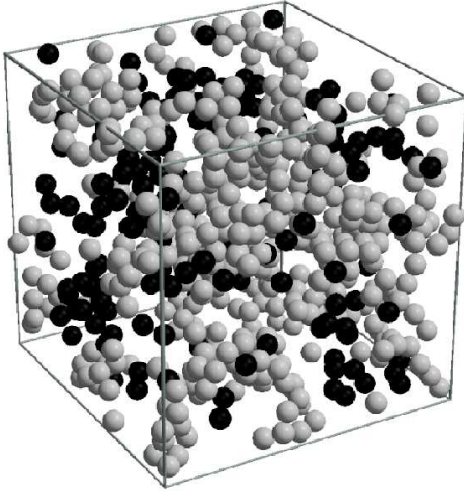


FIG. 4: A snapshot for the gas phase near the coexistence at $T = 0.915$. The light grey and the black spheres represent the gel and fluid particles, respectively. The boxlength is $L = 15$. All quantities are in Lennard-Jones units.

diagram is substantially modified by the presence of the aerogel : both the critical temperature and density are lower than in the bulk and the range of the vapor-liquid coexistence curve is much less extended. We recall that in the bulk the critical parameters are: $T_c = 1.1876$, $\rho_c = 0.3197$ and $\mu_c = -2.778^{29}$.

Our findings about the gas-liquid coexistence properties are in qualitative agreement with previous computer simulation studies on Lennard-Jones fluids confined in random spheres matrices with purely repulsive adsorbent-adsorbate interactions.^{19,20}

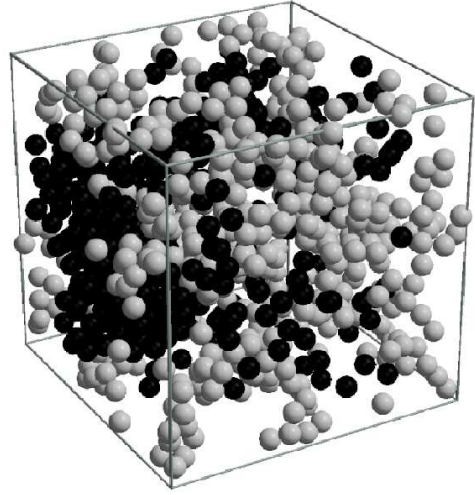


FIG. 5: A snapshot for the liquid phase near the coexistence at $T = 0.915$. The light grey and the black spheres represent the gel and fluid particles, respectively. The boxlength is $L = 15$. All quantities are in Lennard-Jones units.

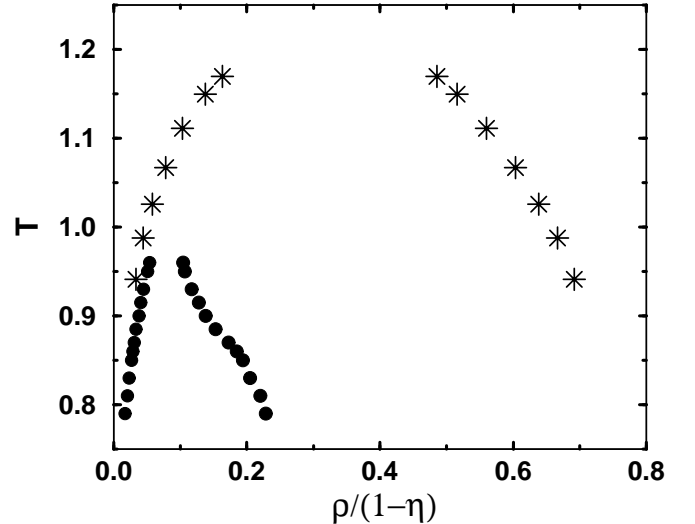


FIG. 6: Phase diagram for the confined fluid obtained from the particle number distribution peak locations (circles) compared with that of the bulk fluid²⁹(stars). All quantities are in Lennard-Jones units.

None-the-less the phase diagram reported in Fig. 6 does not present a liquid-liquid coexistence region. It shows instead a well defined shoulder on the liquid side boundary for intermediate temperatures in the range investigated.

We must however stress that confining primary particles in real aerogels are substantially larger than the

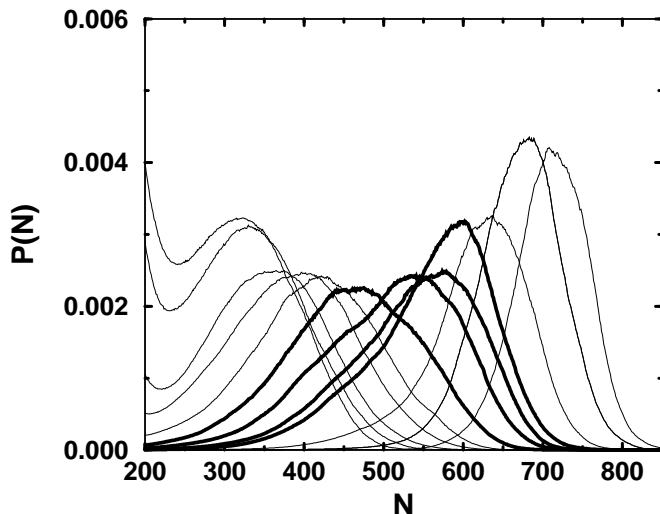


FIG. 7: Blow up of the liquid peaks of the number particles distributions depicted in Fig. 3. The bold solid lines correspond to the liquid peaks generating the observed shoulder in the phase diagram ($T = 0.885$, $T = 0.87$, $T = 0.86$ and $T = 0.85$ in Lennard-Jones units).

fluid molecules, therefore a study on a much larger system could help to shed light on this issue.

In order to better define the nature of the liquid phase for the thermodynamic points corresponding to this shouldering, in Fig 7 we show a blow up of the liquid peaks of the $P(N)$ distributions centered around the intermediate temperature region. The liquid peaks generating the shoulder in the coexistence curve are indicated with bold solid lines. The liquid peaks shape shows a peculiar behavior with varying temperature. For temperatures ranging from near the critical point to about $T = 0.90$, the shape of the liquid peaks is symmetric around the peaks maximum as observed for the bulk²⁹. For the reduced temperature corresponding to the onset of the shoulder, $T = 0.885$ (the first bold curve on the left), the liquid peak shows a bump on its right side that renders its shape slightly asymmetric. We observe that the position of this bump roughly corresponds to the liquid peak maximum of the next $P(N)$ distribution, corresponding to $T = 0.87$. For $T = 0.87$ (the second bold curve starting from the left) it is conversely observed a bump located on the left side of the liquid peak at nearly the same position of the peak maximum measured at $T = 0.885$. We additionally note that the main peaks of these two curves show a more pronounced separation from each other compared with the other curves, in spite of being the temperature jump between one curve and the next approximately similar for all the curves investigated. The next two liquid peaks, corresponding to the end of the shouldering, $T = 0.86$ and $T = 0.85$, are less asymmetric and closer than the two previous ones. For temperatures lower than $T = 0.85$, after the shoulder in the phase diagram, the shape of the liquids peaks

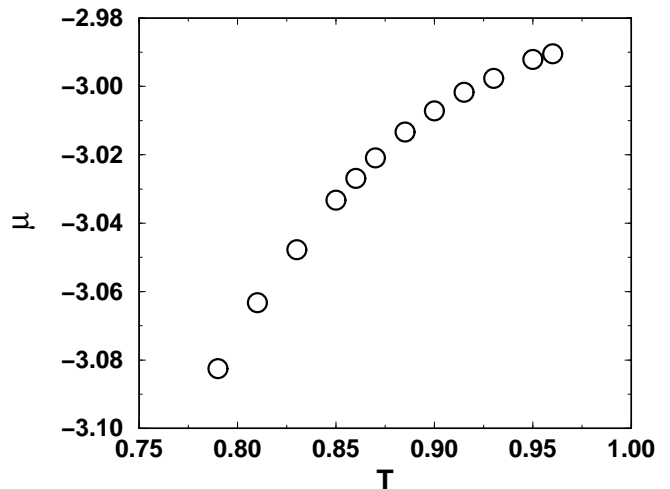


FIG. 8: The confined fluid liquid-gas saturation line in the (μ, T) plane for temperatures ranging from $T = 0.96$ to $T = 0.79$. All quantities are in Lennard-Jones units.

returns to be symmetric and the liquid densities increase regularly on lowering temperature, similar to the high temperatures range.

From these observations we can infer that at high temperatures the gas phase coexists with a medium density liquid. Correspondingly the coexistence curve decreases regularly with temperature. In the intermediate temperature range the liquid phase starts showing high density fluctuations and appears to coexist with a slightly more dense liquid. This region is characterized by an asymmetry in the liquid peaks of the $P(N)$ and correspondingly a shouldering of the phase diagram, that mark a crossover to a slightly more dense phase. For lower temperatures the higher density liquid becomes the thermodynamically favoured phase coexisting with the vapor and the coexistence curve resumes a regular descent.

Finally we report the liquid-vapor coexistence curve in the (μ, T) plane as obtained from our multicanonical simulations. According to the equal peak weight criterion, described in Sec. 3, the location of the liquid-vapor saturation line in this plane can be obtained looking for the values of temperature and chemical potential at which the bimodal distributions $P(N)$ have equal area under the two peaks.

Fig. 8 shows the temperature behavior of the coexistence chemical potentials at which we obtained the $P(N)$ distributions reported in Fig. 3. Analogous to the bulk we observe a monotonic regular behavior. Similar to the temperature versus density phase diagram, there is a substantial shrinkage of the range of chemical potentials at which we observe the coexistence of the liquid and gas phases with respect to the bulk. In fact in the bulk²⁹ for a similar interval of temperatures as ours, i.e. $\Delta T = 0.17$, a range $\Delta\mu \sim 0.6$ is found, while in our confined system $\Delta\mu \sim 0.09$, more than six times lower.

V. CONCLUSIONS

We have performed a computer simulation study of the phase behavior of a Lennard-Jones fluid adsorbed in a highly porous fractal aerogel. The gel environment has been generated with the DLCA algorithm^{25,27} in order to obtain a more realistic confining structure than those reported in literature. Besides the confined fluid phase diagram has been calculated by performing multicanonical ensemble simulations in the framework of the Monte Carlo grand canonical ensemble technique^{28,29,30}.

The proper bias has been found by applying the single-histogram reweighting technique³³. This procedure is particularly suitable for analysing the transition state of the first order phase transitions in great detail.

We found that the phase diagram of the confined fluid is substantially modified with respect to the bulk by the presence of the gel: the critical temperature and density are lower and the liquid-gas coexistence curve is much narrower than in the bulk. Our findings about the vapor-liquid coexistence properties are in qualitative agreement with experimental observations and previous theoretical studies. We have not found a clear evidence for a second liquid-liquid coexistence region in the fluid phase diagram. The presence of a liquid-liquid phase coexistence has been sometimes reported, depending on the particular configuration generated for the adsorbent, random matrices of spheres^{19,20}. Our coexistence curve shows a shoulder on the liquid side boundary in the intermediate temperature range. For the same temperatures the liquid peaks shape of our particles number distributions

are highly asymmetric and show a bump. However, since we do not find two distinctly resolved peaks, we must conclude that in our case coexistence between two liquid phases is never observed. We do observe instead a crossing of the liquid from a lower to an higher density phase upon decreasing temperature.

We have employed in this study a very sophisticated technique for an accurate location of the coexistence curve. Due to the fractal structure of the confining environment the results should in principle not depend on the realization. However we cannot exclude that finite size effects could be present. Only extensive analysis with increasing sizes can confirm how sensitive the results are to the matrix realization.

In order to gain deep insight about the modification of the phase diagram of fluids confined in aerogels the modeling of the adsorbent environment can be further improved to make contact with the experimental situations. It would be interesting to explore in a more carefully designed confining structure with a network of multishaped voids if the two liquid phases will become distinguishable. In particular the liquid-liquid coexistence is smeared out in our present simulation, where we observe only a shouldering in the phase diagram. It would be valuable to perform simulations on even larger systems to better investigate the role of the fractal behavior of the confining medium and perform an extensive analysis of finite size effects.

Work on these improvements to our present study is currently in progress.

-
- ¹ L. D. Gelb, K. E. Gubbins, R. Radhakrishnan and M. Sliwinska-Bartkowiak Rep. Prog. Phys. **62**, 1573 (1999).
 - ² J. V. Maher, W. I. Goldburg, D. W. Pohl and M. Lanz Phys. Rev. Lett. **53**, 60 (1984).
 - ³ A. P. Y. Wong and M. H. W. Chan Phys. Rev. Lett. **65**, 2567 (1990).
 - ⁴ B. J. Frisken, F. Ferri and D. S. Cannell Phys. Rev. Lett. **66**, 2754 (1991).
 - ⁵ B. J. Frisken and D. S. Cannell Phys. Rev. Lett. **69**, 632 (1992).
 - ⁶ A. P. Y. Wong, S. B. Kim, W. I. Goldburg and M.H.W. Chan Phys. Rev. Lett. **70**, 954 (1993).
 - ⁷ B. J. Frisken, F. Ferri and D. S. Cannell Phys. Rev. E **51**, 5922 (1995).
 - ⁸ S. B. Dierker and P. Wiltzius Phys. Rev. Lett. **58**, 1865 (1987).
 - ⁹ D. Finotello, K. A. Gillis, A. Wong and M. H. W. Chan Phys. Rev. Lett. **61**, 1954 (1988).
 - ¹⁰ P. Wiltzius, S. B. Dierker and B. S. Dennis Phys. Rev. Lett. **62**, 804 (1989).
 - ¹¹ S. B. Dierker and P. Wiltzius Phys. Rev. Lett. **66**, 1185 (1991).
 - ¹² N. J. Wilkinson, M. A. Alam, J. M. Clayton, R. Evans, H. M. Fretwell and S. G. Usmar Phys. Rev. Lett. **69**, 3535 (1992).
 - ¹³ M. Y. Lin, S. K. Sinha, J. M. Drake, X. -I. Wu, P. Thiagarajan and H.B. Stanley Phys. Rev. Lett. **72**, 2207 (1994).
 - ¹⁴ F. Brochard and P. G. de Gennes, J. Phys. (France) Lett. **44**, 785 (1983); P.G. de Gennes, J. Phys. Chem. **88**, 6469 (1984).
 - ¹⁵ W. G. Madden and E. D. Glandt J. Stat. Phys. **51**, 537 (1988); W. G. Madden J. Chem. Phys. **96**, 5422 (1992).
 - ¹⁶ E. Kierlik, M. L. Rosinberg, G. Tarjus and P. A. Monson J. Chem. Phys. **106**, 264 (1997).
 - ¹⁷ V. Krakoviack, E. Kierlik, M. L. Rosimberg and G. Tarjus J. Chem. Phys. **115**, 11289 (2001).
 - ¹⁸ M. Cieplak, A. Maritan, M. R. Swift, F. Toigo and J. R. Banavar Phys. Rev. E **66**, 056124 (2002).
 - ¹⁹ K. S. Page and P. A. Monson Phys. Rev. E **54**, R29 (1996); K. S. Page and P. A. Monson Phys. Rev. E **54**, 6557 (1996).
 - ²⁰ M. Alvarez, D. Levesque and J. J. Weis Phys. Rev. E **60**, 5495 (1999).
 - ²¹ L. Sarkisov and P. A. Monson Phys. Rev. E **61**, 7231 (2000).
 - ²² D. W. Schaefer and K. D. Keefer, Phys. Rev. Lett. **56**, 2199 (1986).
 - ²³ T. Freltoft, J. K. Kjems and S. K. Sinha Phys. Rev. B **33**, 269 (1986).
 - ²⁴ A. Hasmy, M. Foret, J. Pelous and R. Jullien Phys. Rev. B **48**, 9345 (1993).

- ²⁵ A. Hasmy, E. Anglaret, M. Foret, J. Pelous and R. Jullien *Phys. Rev. B* **50**, 6006 (1994).
- ²⁶ A. Hasmy, R. Vacher and R. Jullien *Phys. Rev. B* **50**, R1305 (1994).
- ²⁷ M. Kolb and H. Herrmann *J. Phys. A* **18**, L435 (1985).
- ²⁸ B. A. Berg and T. Neuhaus *Phys. Rev. Lett.* **68**, 9 (1992).
- ²⁹ N. B. Wilding *Phys. Rev. E* **52**, 602 (1995).
- ³⁰ N. B. Wilding *Am. J. Phys.* **69**, 1147 (2001).
- ³¹ M. P. Allen and D. J. Tildesley *Computer Simulation of Liquids* Oxford University Press (1987).
- ³² D. Frenkel and B. Smit *Understanding Molecular Simulations* Academic Press, Boston (1996).
- ³³ A. M. Ferrenberg and R. H. Swendsen *Phys. Rev. Lett.* **61**, 2635 (1988); A. M. Ferrenberg and R. H. Swendsen *Phys. Rev. Lett.* **63**, 1195 (1989); A. M. Ferrenberg and R. H. Swendsen *Computers in Physics* **3**(5), 101 (1989).
- ³⁴ E. Kierlik, P. A. Monson, M. L. Rosinberg, L. Sarkisov and G. Tarjus *Phys. Rev. Lett.* **87**, 055701 (2001).